Cite as: J. Appl. Phys. 133, 214101 (2023); doi: 10.1063/5.0146059

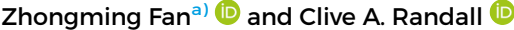
Submitted: 9 February 2023 · Accepted: 16 May 2023 ·

Published Online: 1 June 2023











Materials Research Institute, Pennsylvania State University, University Park, Pennsylvania 16802, USA

a)Author to whom correspondence should be addressed: zbf5066@psu.edu

### **ABSTRACT**

Adding excessive metal oxide doping to a powder batch is a known way to compensate for the loss of volatile cation species during high temperature sintering. An important case in the piezoelectric ceramics is the bismuth oxide in the lead-free ferroelectric ceramic bismuth sodium titanate (BNT). Building from the earlier knowledge about excessive bismuth oxide's influences on the properties of BNT, we further note that varying the sintering temperature can both control the distribution of excessive Bi3+ and impact the relaxor/normal ferroelectric behaviors and corresponding phase transition. In addition to the nature of polarization, the sintering temperature also significantly manipulates the electrical conductivity. A hypothetical mechanism for the resistive grain boundary is proposed, based on inferences from electrical—microstructure—processing relations in 85% Bi<sub>0.5</sub>Na<sub>0.5</sub>TiO<sub>3</sub>-15% BaTiO<sub>3</sub> with batched Bi<sub>2</sub>O<sub>3</sub> excess and acceptor Mg<sup>2+</sup> in a codoped strategy.

Published under an exclusive license by AIP Publishing. https://doi.org/10.1063/5.0146059

### I. INTRODUCTION

Bi<sub>0.5</sub>Na<sub>0.5</sub>TiO<sub>3</sub> (BNT) is one of the lead-free candidates to potentially replace the lead containing piezoelectric ceramics. BNT has some shortcomings such as the magnitude of piezoelectric properties and the limited temperature range.2 However, BNT ceramics can readily achieve good densification and electrical insulation. As BNT drives toward commercialization, a better understanding of Bi3+ non-stoichiometry is of increasing importance. In BNT, the bismuth vacancies are usually compensated by ionic oxygen vacancies, according to the following equation:

$$2Bi_{Bi}^{\times} + 3O_O^{\times} \stackrel{BNT}{\rightarrow} 2V_{Bi}^{\prime\prime\prime} + 3V_O^{\cdot\cdot} + a(Bi_2O_3), \tag{1}$$

preventing the high dielectric loss until elevated temperatures.<sup>3</sup> Here, we use the Kroger-Vink notation, and "a" is the activity of Bi<sub>2</sub>O<sub>3</sub>. Furthermore, the large amount of oxygen vacancies produced by bismuth volatility naturally limits long-term reliability of

BNT-based materials operating under a direct or pulsed unipolar

Earlier, Sinclair's group has shown that undoped BNT exhibits high ionic conductivity, while batched with 2 at. % excess, Bi<sub>2</sub>O<sub>3</sub> (B<sub>0.51</sub>NT) could significantly suppress ionic conduction.  $(B_{0.51}NT)$  could significantly suppress ionic conduction. Conceivably, the excess  $Bi_2O_3$  compensates for evaporated  $Bi_2O_3$ , thereby suppressing Eq. (1). However, the excess Bi<sub>2</sub>O<sub>3</sub> could also  $\Xi$ theoretically serve as a donor dopant for A-site once it occupies a sodium vacancy. This competition of A-site occupancy accounts for ionic conduction that is enhanced by the introduction of excess sodium oxide into the BNT system: excessive Na<sup>+</sup> entering bismuth vacancies becomes an acceptor dopant that in turn can create more oxygen vacancies.<sup>5</sup> Therefore, the excess Bi<sub>2</sub>O<sub>3</sub> should not only influence the electrical conductivity by compensating for evaporation, but it is also able to impact the polar nature when it plays the role of a donor dopant. There have been many papers that discussed the relation between A-site non-stoichiometry and the ferroelectric behaviors in BNT.<sup>6-8</sup> In this paper, our objective was to identify other correlated properties that are unique to BNT

compositions with batched  $\rm Bi_2O_3$  excess. Here, we select the solid solution 85%  $\rm Bi_{0.5}Na_{0.5}TiO_3$ -15%  $\rm BaTiO_3$  (BNT-15BT) to demonstrate these trends with sintering temperature and non-stoichiometry.

## II. EXPERIMENTAL

The BNT-15BT ceramics were fabricated using a conventional solid state reaction method, with starting powders of  $\rm Bi_2O_3$  (>99.9%),  $\rm Na_2CO_3$  (>99.95%),  $\rm TiO_2$  (>99.9%),  $\rm BaCO_3$  (>99.8%), and MgO (>99.99%) weighted according to the stoichiometry. The mixed powders were ball milled in ethanol both before and after calcination. The calcined powder, mixed with 1.5 wt. % Acryloid binder, was pressed into a 15 mm diameter disk prior to sintering. The binder was then burned out at 600 °C for 2 h. Both calcination and sintering were conducted for 2 h with a 5 °C/min heating and

cooling rate, while the temperatures are subject to change as will be explained in detail. The as sintered pellets were polished to ~1 mm in thickness before platinum electrodes were sputtered. The x-ray diffraction pattern was collected by Empyrean (PANalytical, UK). The impedance spectroscopy was performed in a computercontrolled furnace with a Solartron ModuLab XM impedance analyzer from 0.1 Hz to 1 MHz. The polarization-field (P-E) hysteresis loop was recorded using a Sawyer-Tower circuit with a Trek Model 30/20 high voltage amplifier system (Trek, Inc., Lockport, NY). The depolarization temperature was identified via the pyroelectric measurement based on a modified Byer and Roundy setup equipped with a pA meter (4140B, Hewlett Packard). The microstructure in the ceramics was checked with transmission electron microscopy (TEM) on Talos F200X (FEI). Energy dispersive x-ray spectroscopy (EDS) mapping was acquired by a SuperX EDX detector. The TEM specimens were prepared by a focused ion beam (Scios, FEI).

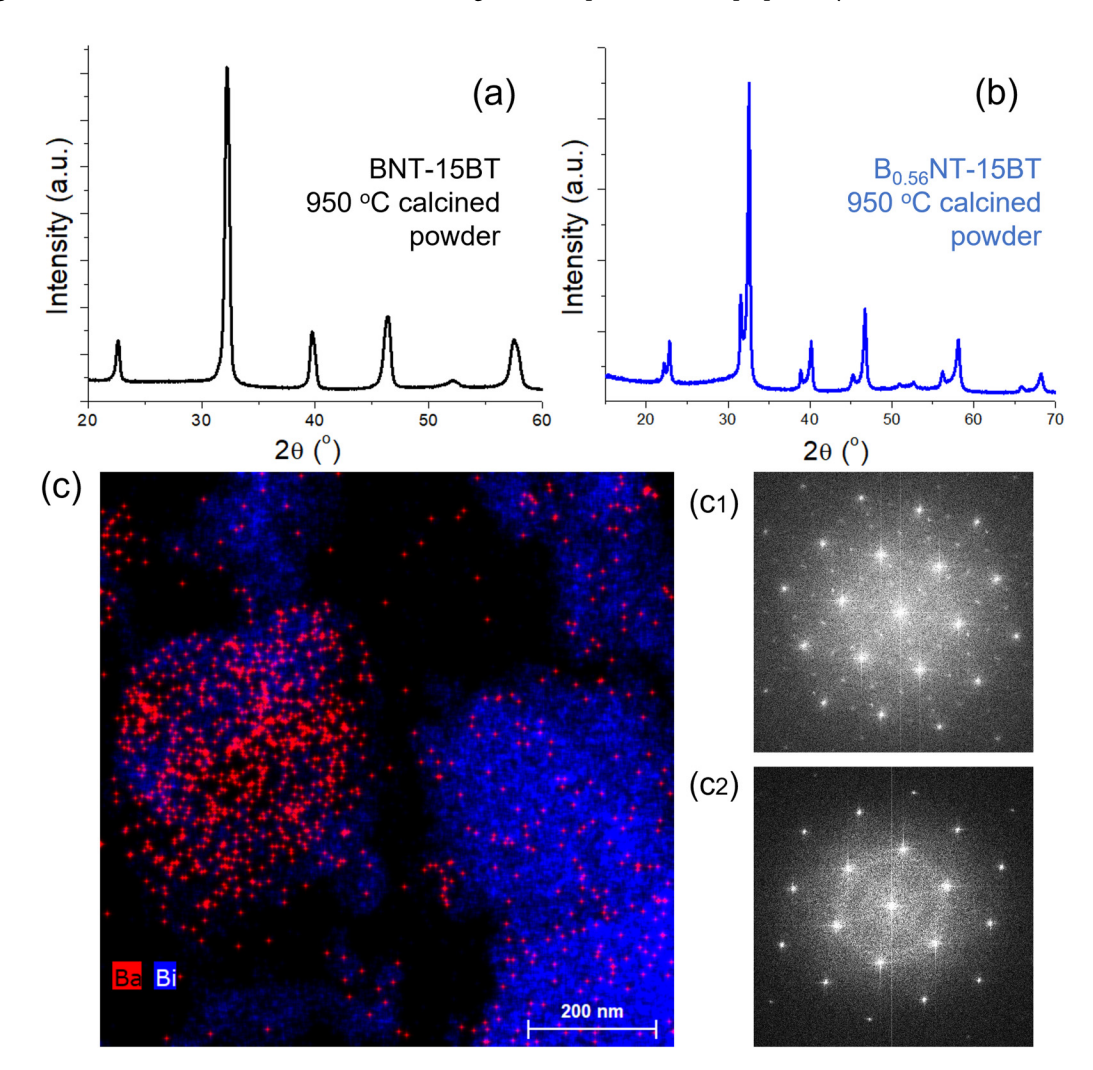


FIG. 1. Powder x-ray diffraction pattern of the 950 °C calcined (a) BNT-15BT and (b) B<sub>0.56</sub>NT-15BT. (c) STEM-EDS mapping of the 950 °C calcined B<sub>0.56</sub>NT-15BT powder, with the electron diffraction pattern of a (c<sub>1</sub>) BNT-BT and (c<sub>2</sub>) BTO powder.

## **III. RESULTS AND DISCUSSION**

The thermal processes of solid-state calcination and sintering are essential to the final ceramics' performance. Typically, it is found that most publications report calcination <950 °C followed by sintering < 1200 °C of BNT-BT ceramics. 9,10 Figure 1(a) shows that calcining the stoichiometric raw powders at 950 °C does lead to a single perovskite phase. However, the powders with 12% excess Bi<sub>2</sub>O<sub>3</sub>, namely, B<sub>0.56</sub>NT-15BT, do not form a single phase after a 950 °C calcination process [Fig. 1(b)]. The XRD pattern suggests two perovskite phases' coexistence under these conditions with two lattice parameters. The two phases are further confirmed under an EDS-STEM observation [Fig. 1(c)]. The 1/2{ooe} superlattice spots in the electron diffraction pattern from a BNT-BT particular indicates a P4bm (tilted oxygen octahedra) rather than the reported and expected P4mm (no tilting) symmetry  $(c_1)$ . The second perovskite phase having larger lattice parameter is BaTiO<sub>3</sub>, where there is no tilted structure and superlattices (c2). Despite all the Bi2O3 excess, no Bi<sub>2</sub>O<sub>3</sub> phases are present in the calcined powder, but

instead, BaTiO3 is generated from the solid-state reaction. It implies that Bi<sub>2</sub>O<sub>3</sub> ions may have accommodated the A-site of BNT and in doing so rejecting some Ba<sup>2+</sup> ions. The calcination temperature was then raised from 950 to 1000 °C. Figure 2(a) shows that the higher temperature calcined powder does not contain as much BaTiO<sub>3</sub>, implying there is more incorporation of Ba<sup>2+</sup> into the BNT-BT main phase, and there is still no Bi<sub>2</sub>O<sub>3</sub> secondary phase as noted on the XRD. On closer examination of the XRD peak, it is two peaks merging together, the one at a higher Bragg angle is likely rich in Bi<sup>3+</sup> relative to Ba<sup>2+</sup> at its A-site as Bi<sup>3+</sup> is smaller in size. In other words, the excess Bi<sub>2</sub>O<sub>3</sub> remains "doped" in the perovskite lattice. Our observations agree with the previous in situ XRD data, in which Jones and co-workers have found intensified  ${\rm BaTiO_3}$  secondary phase in the BNT-BT with higher Ba content.  $^{11,12}$  The  ${\rm BaTiO_3}$  is a product of the reaction between  ${\rm TiO_2}$ and BaCO<sub>3</sub> starting from 650 °C, which will not disappear until obtaining temperatures of  $\sim 1000$  °C.  $^{12}$  Note that these previous works were done in the stoichiometry situation, and our Bi excess case could provide more insights into the phase formation

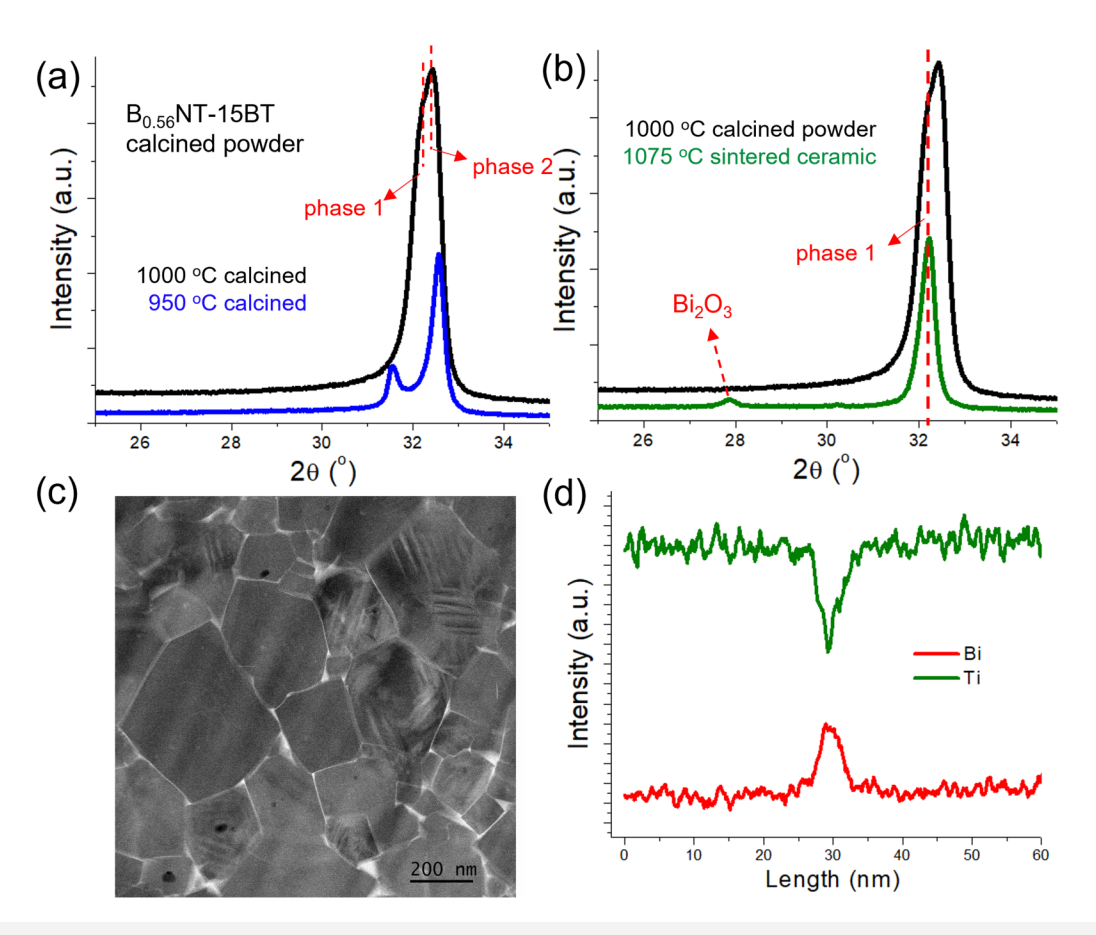


FIG. 2. (a) The x-ray powder diffraction patterns of B<sub>0.56</sub>NT-15BT calcined at 950 and 1000 °C; the 950 °C powder has BTO secondary phase; the 1000 °C powder also contains two phases: phase 1 is stoichiometric, whereas phase 2 is rich in Bi<sup>3+</sup> in relative to Ba<sup>2+</sup>. (b) The x-ray diffraction pattern from the 1075 °C sintered ceramic using 1000 °C calcined powder, phase 2 disappears while Bi<sub>2</sub>O<sub>3</sub> secondary phase appears. (c) STEM image of the 1075 °C sintered ceramic using 1000 °C calcined powder, and the intergranular brighter contrast is Bi<sub>2</sub>O<sub>3</sub>. (d) The EDS line profile across a grain boundary showing the presence of a thin layer of Bi<sub>2</sub>O<sub>3</sub>.

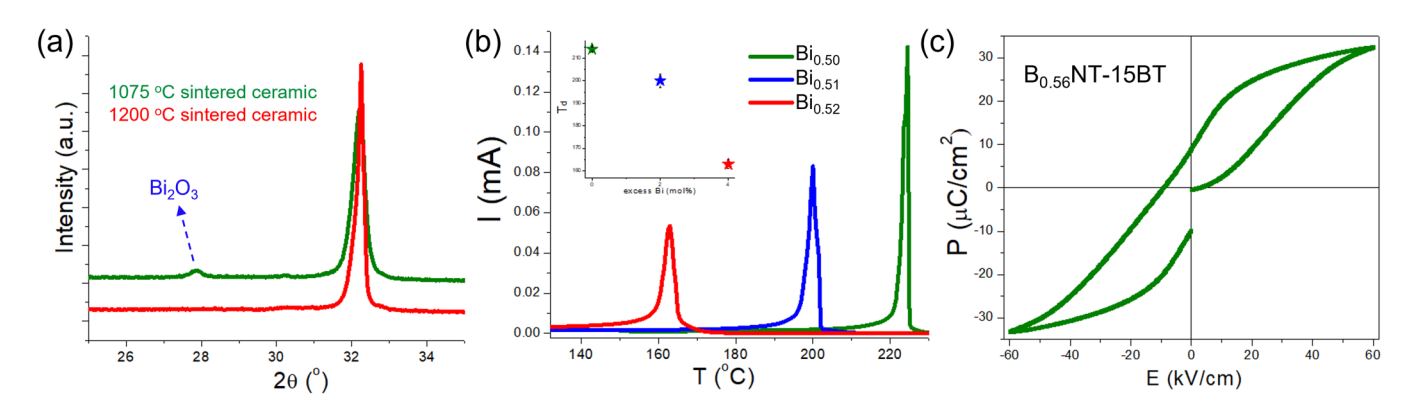


FIG. 3. (a) X-ray diffraction patterns of the B<sub>0.56</sub>NT-15BT ceramics sintered at 1075 and 1200 °C, and no Bi<sub>2</sub>O<sub>3</sub> secondary phase in the 1200 °C sintered sample. (b) Pyroelectric measurements conducted in poled ceramics, showing the decrease in T<sub>d</sub> as a function of Bi<sup>3+</sup> excess. (c) P-E loop measured from 1200 °C sintered B<sub>0.56</sub>NT-15BT samples at room temperature.

mechanism of BNT-BT. It was previously hypothesized that Bi<sub>2</sub>O<sub>3</sub> serves as a host for other reactants to diffuse in, converting to the final BNT.11 Our results with non-stoichiometric batching seem to support this hypothesis. If the reaction occurs between the reactants at the particle contacting surface, the excessive Bi<sub>2</sub>O<sub>3</sub> is likely left. So, with the observation of no Bi<sub>2</sub>O<sub>3</sub> secondary phases, we infer there is a final stage. This is the incorporation of excessive Bi<sup>3+</sup> ions into the A-site, thereby preventing the transient BaTiO<sub>3</sub> phase from being incorporated.

Subsequently, the 1000 °C calcined powder was sintered at 1075 °C, a temperature lower than what is commonly used. In these ceramics, the Bi<sub>2</sub>O<sub>3</sub> secondary phase appears while the phase with smaller lattice parameter, which formerly incorporates the excessive Bi<sup>3+</sup>, disappears [Fig. 2(b)]. The STEM imaging in Fig. 2(c) illustrates that the Bi<sub>2</sub>O<sub>3</sub> secondary phase is dispersed at grain boundaries, forming an intergranular layer with a thickness of ~5 nm [Fig. 2(d)]. The Bi<sub>2</sub>O<sub>3</sub>, being released and activated as a sintering aid, enables the densification to occur at relatively low temperatures. The microstructure observed here resembles that in the Bi<sub>2</sub>O<sub>3</sub>-based ceramics sintered at around 1000 °C. <sup>13</sup> The difference. BiFeO<sub>3</sub>-based ceramics sintered at around 1000 C. The list that the calcined BiFeO<sub>3</sub> powder already contains impurity on the intergranular phase is "created" by the intergranular phase is "created" on the BiFeO<sub>3</sub>-based ceramics sintered at around 1000 °C. <sup>13</sup> The difference under the sintering process.

When the  $B_{0.56}NT-15BT$  ceramic is sintered at 1200 °C, the  $\frac{5}{6}$ lattice parameter of the perovskite phase is almost identical with the low temperature sintered samples, whereas the Bi<sub>2</sub>O<sub>3</sub> secondary phase no longer exists [Fig. 3(a)]. There could be two possibilities

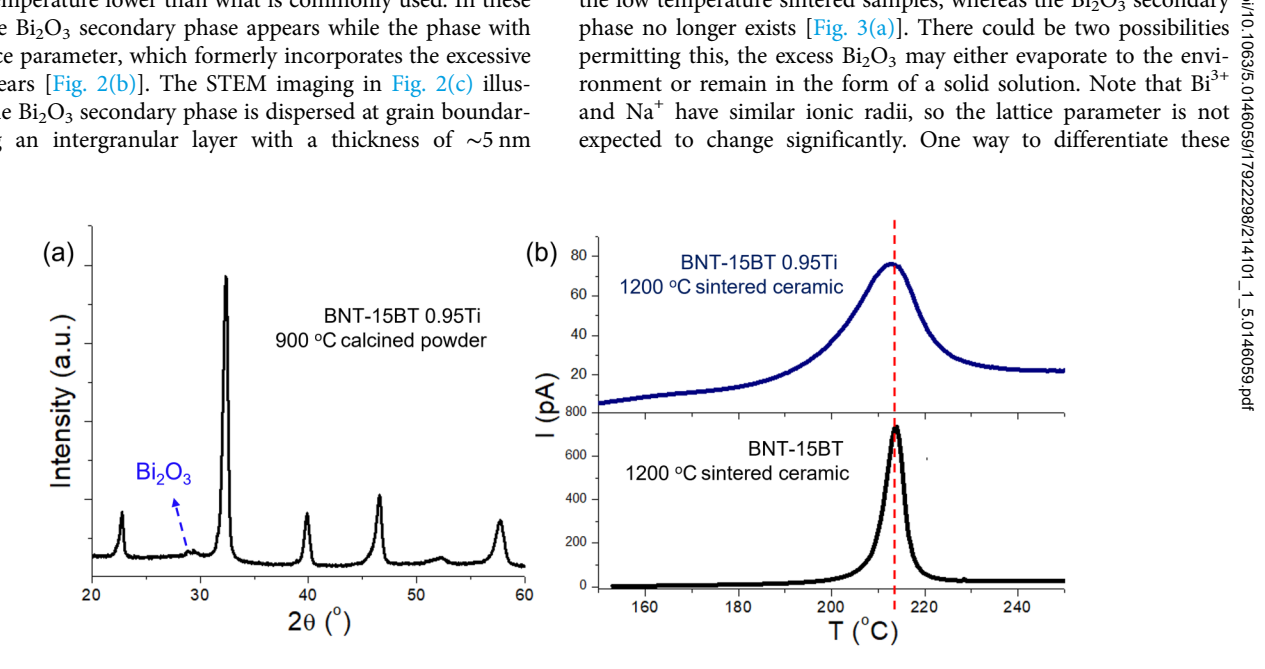


FIG. 4. (a) X-ray powder diffraction pattern of the BNT-15BT 0.95Ti calcined at 900 °C, containing the Bi<sub>2</sub>O<sub>3</sub> secondary phase. (b) Pyroelectric measurements conducted in unpoled ceramics, showing the insensitivity of T<sub>d</sub> to the Ti<sup>4+</sup> deficiency.

scenarios is to investigate the ferroelectric properties that are generally sensitive to the defect chemistry. 14,15 So, if the batched excess Bi<sub>2</sub>O<sub>3</sub> evaporates into the atmosphere of the furnace, we would expect the ferroelectric properties to remain invariant relative to a stoichiometric BNT-15BT material. If, on the other hand, there is a solid solution incorporation of excess Bi<sub>2</sub>O<sub>3</sub>, the ferroelectric properties would vary as a function of bismuth content. The pyroelectric peak current can be used to conveniently monitor the depolarization temperature when T<sub>d</sub> is higher than the room temperature. From the TSDC data measured in the poled samples with various non-stoichiometries, we note a systematic decrease with increasing excess Bi<sub>2</sub>O<sub>3</sub> [Fig. 3(b)]. The T<sub>d</sub> in B<sub>0.56</sub>NT-15BT is supposed to further decrease to around room temperature. We deduced this not from TSDC because it is unable to unambiguously reveal the pyroelectric peak under this circumstance but from the P-E hysteresis loop measured at room temperature where we noticed an apparently suppressed remanent polarization relative to maximum polarization [Fig. 3(c)]. 16 Given the continuous drop of  $T_d$  with  $Bi^{3+}$  content, we believe that the excess  $Bi_2O_3$  are incorporated in a non-stoichiometric solid solution, and the evaporated content is less important, when sintered at 1200 °C.

In contrast, through a Ti deficient batching, that one may anticipate is analogous to Bi excess batching, this is found not to be the case. Figure 4(a) shows the powder diffraction pattern of the calcined BNT-15BT with 5% Ti<sup>4+</sup> deficiency. Interestingly, in this processing route, a secondary bismuth oxide phase is observed in the XRD data. When sintered at relatively low temperatures (1000 °C), the bismuth oxide resides as an intergranular phase, forming a microstructure as represented in the TEM micrograph in Fig. 2(c). When sintered at relatively higher temperatures (1200 °C), the bismuth oxide secondary phase again disappears. However, in this case, the T<sub>d</sub> barely changes compared to the stoichiometry sample [Fig. 4(b)]. Note that the TSDC data here are measured from unpoled samples, since the unpoled ferroelectric state still displays small but distinct macroscopic asymmetry. Therefore, we infer there is no solid solution formation, just as evaporation loss for the redundant Bi<sub>2</sub>O<sub>3</sub>.

According to the observations noted here from Figs. 2 and 3, §

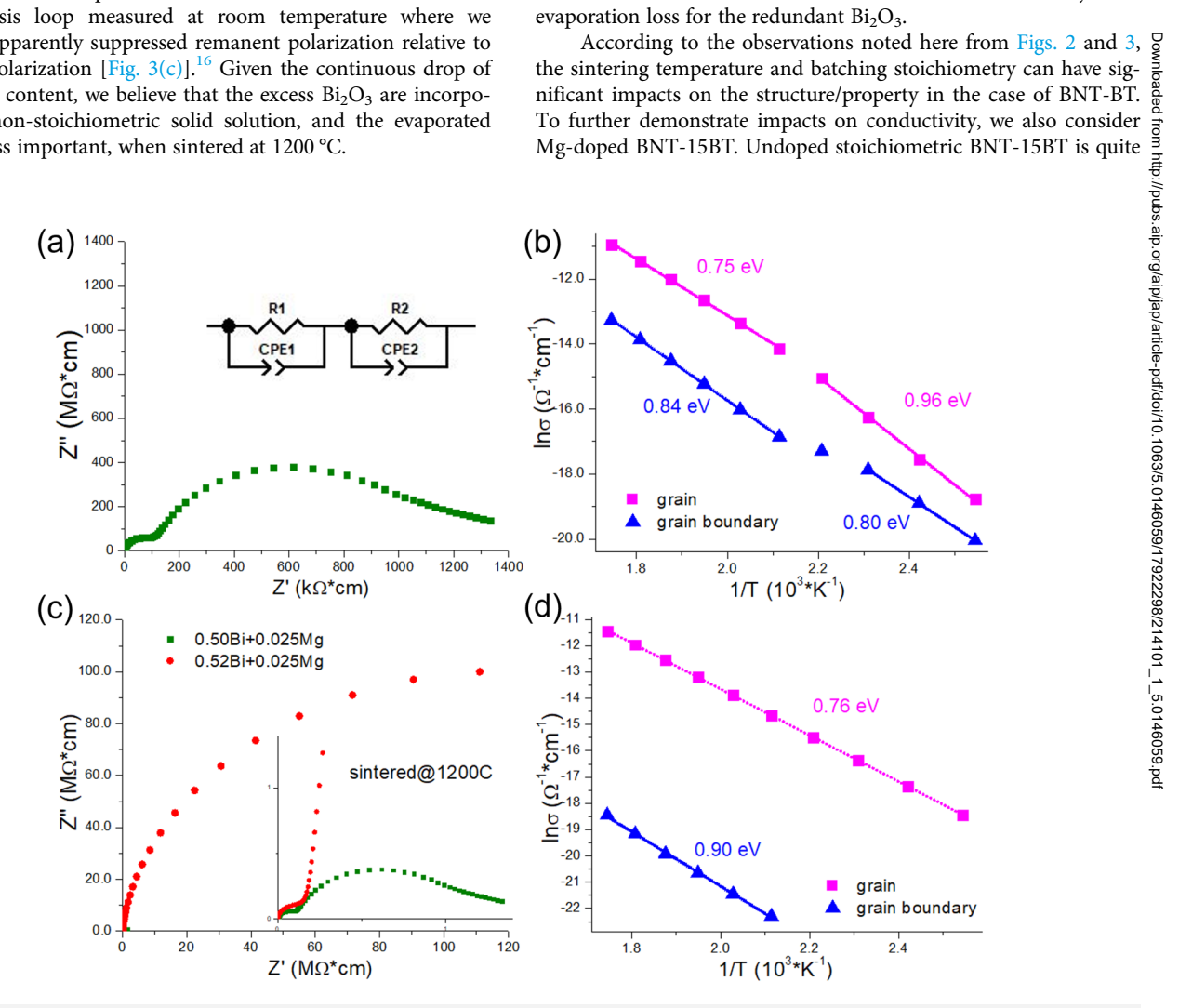


FIG. 5. (a) Impedance spectroscopy measured in 1200 °C sintered stoichiometric BNT-15BT 0.025 Mg ceramic, the corresponding Arrhenius plot of the grain and grain boundary conductivity in (b). (c) Comparison of conductivities in the 1200 °C sintered BNT-15BT 0.025 Mg ceramics with and without Bi3+ excess. (d) Arrhenius plot of the grain and grain boundary conductivity in 1200 °C sintered BNT-15BT 0.025 Mg ceramic with Bi3+ excess.

insulating owing to the absence of significant ionic conduction. <sup>4</sup> The Mg<sup>2+</sup> doping makes BNT-15BT much more ionic conductive via creating oxygen vacancies through ionic compensation, in accordance to Eq. (2),

$$MgO \xrightarrow{BNT} Mg_{Ti}'' + O_O^{\times} + V_O^{\cdot \cdot}.$$
 (2)

The impedance spectroscopy consists of two semicircles, relating to two relaxation mechanisms, the high frequency response originates from the grain response, while the low frequency one represents the grain boundary contribution. The grain boundary resistivity is about one order of magnitude more than the grain, as shown in Fig. 5(b). The Arrhenius plot for the grain conductivity is found divided into two sections with distinct activation energies, implying two mechanisms of phases. The activation energy below ~210 °C is

 ${\sim}0.96\,\mathrm{eV},$  which reduces to  ${\sim}0.75\,\mathrm{eV}$  at higher temperature. In accordance with our previous report, these two activation energies are consistent with oxygen vacancy migration in normal and relaxor ferroelectric phase, respectively. Therefore, Mg²+doped BNT-15BT undergoes a normal to relaxor ferroelectric phase transition upon heating, and the phase transition temperature, or  $T_{\rm d}$ , is around 210 °C. It should be noted that, compared to undoped BNT-15BT [Fig. 3(c)],  $T_{\rm d}$  is barely shifted by Mg²+doping.

Next, we combine the impact of excess  $Bi_2O_3$  and the Mg doping BNT-15BT. Since the excess  $Bi_2O_3$  will be expected to behave as the donor dopant on the perovskite A site when sintered at high temperature as illustrated above, it is under a co-doping scenario able to also compensate for the acceptor charge of  $Mg_{Ti}^{\prime\prime}$ . So, if this is the case, we would further anticipate a suppression of oxygen vacancy concentration and thereby the ionic conductivity

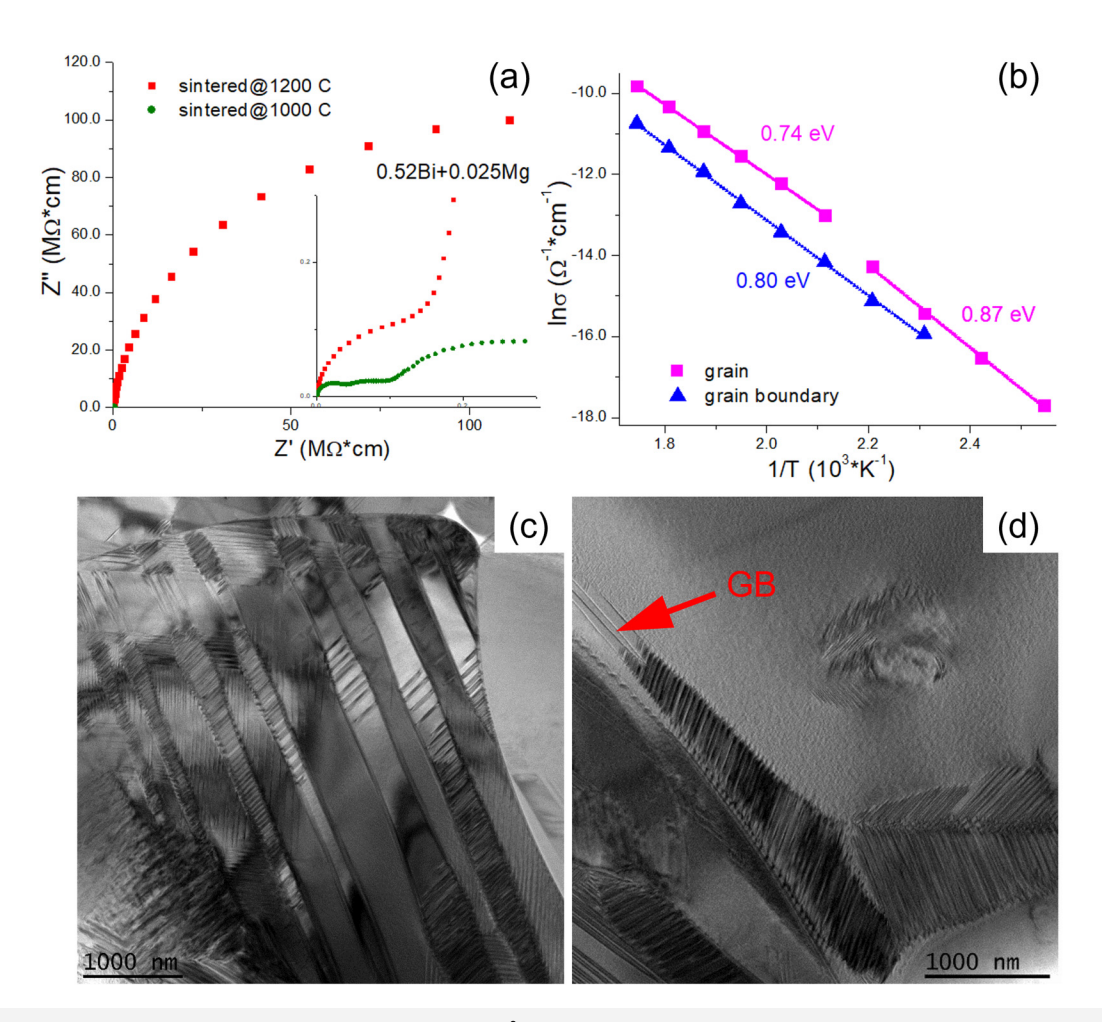


**FIG. 6.** (a) Comparison of conductivities in BNT-15BT 0.025 Mg ceramic with Bi<sup>3+</sup> excess sintered at 1200 and 1000 °C. (b) Arrhenius plot of the grain and grain boundary conductivity in 1000 °C sintered BNT-15BT 0.025 Mg ceramic with Bi<sup>3+</sup> excess. (c) The domain morphology in 1000 °C sintered BNT-15BT 0.025 Mg ceramic with Bi<sup>3+</sup> excess. (d) The domain morphology in 1200 °C sintered BNT-15BT 0.025Mg ceramic with Bi<sup>3+</sup> excess. A grain boundary is highlighted, near which long-range ferroelectric domains are present.

[Eq. (3)]. However, we

$$[Bi_{A}^{\cdot}] + 2[V_{O}^{\cdot}] \approx 2[Mg_{Ti}''],$$
 (3)

see that the grain conductivity is almost unaffected, but the grain boundary resistivity is significantly increased by four orders of magnitude [Fig. 5(c)]. The Arrhenius plot in Fig. 5(d) shows in the co-doped case that there is no slope change associated with a change in the polarization mechanism with temperature in the grain. The activation energy for ionic conduction within the grain is uniformly ~0.76 eV, indicative of the transport within a nonergodic relaxor phase. We also note that the conduction properties of Mg<sup>2+</sup>-doped BNT-15BT ceramic can be dramatically changed by reducing the sintering temperature from 1200 to 1000 °C. At low temperatures, both the grain and grain boundary become more conductive, as shown in Fig. 6(a). More interestingly, perturbation to the grain conductivity reappears in the Arrhenius plot [Fig. 6(b)], around the same temperature as the stoichiometric Mg-doped BNT-15BT [Fig. 5(b)]. The respective activation energies associated with temperature regimes would also indicate a low temperature normal ferroelectric phase and higher temperature relaxor phase. From a TEM study, we can determine the domain morphologies. The low temperature sintered ceramic shows at room temperature large ferroelectric twin domains' configurations [Fig. 6(c)]. In the high temperature sintered sample, the major portion of a grain is filled with nanosized polar nanoregions, typical of a relaxor ferroelectrics [Fig. 6(d)]. The domain configurations in both cases coincide with the expected phases inferred from Arrhenius plots. The mechanism behind this dramatic change is believed to be associated with the dependence of Bi<sub>2</sub>O<sub>3</sub> distribution impacted from sintering temperature. In the low temperature sintered sample, the ferroelectric phase nature, including T<sub>d</sub>, is hardly influenced relative to the stoichiometry case due to the fact that the excess Bi<sub>2</sub>O<sub>3</sub> is located at the grain boundary rather than doped in the grain. However, when sintered at a high temperature of ~1200 °C, the excess Bi<sub>2</sub>O<sub>3</sub> remains doped in the bulk grain phase. This destabilizes the long-range ferroelectric ordering, decreases the T<sub>d</sub>, and transitions the bulk of the grain to a relaxor system. Consequently, the high temperature sintered samples become nonergodic relaxor phase at room temperature.

Finally, we must also consider the grain boundary resistivity enhancement in the high temperature sintered sample [Figs. 5(c) and 5(d)]. It should be noted that despite the relaxor phase and a nanosized domain contrast in the bulk of the grains, there exist long-range normal ferroelectric twin domain structures near the grain boundaries [Fig. 6(d)]. In principle, we noted that oxygen vacancy migration is more difficult in the normal ferroelectric phase than in the relaxor phase. However, the observed four-order-of-magnitude difference in grain boundary conductivity is too significant to be solely explained by the microstructure, so there is likely a compositional contribution. The contrast between the domain configuration close to and away from the grain boundary suggests that the grain boundary region has higher T<sub>d</sub> than the grain interior. As excess Bi<sub>2</sub>O<sub>3</sub> doping on the A-site decreases the T<sub>d</sub>, the grain interior rather than the grain boundary region would be more heavily doped. So, the resistive grain boundary region may be comparably depleted in all point defects, as it

undergoes high temperature sintering, likely in accordance to Eq. (3). In other words, we speculate that the grain boundary region is compositionally closer to an undoped stoichiometric BNT-15BT, which shows predominantly electronic conduction, hence much more insulating than ionically conductive bulk grain interiors. Usually, the acceptor cations would segregate in the grain boundary region in many acceptor-doped ceramics, forming a depletion shell that prevents the transgranular transport of oxygen vacancies. 17, This common mechanism could in principle readily find the support from EDS data. However, in our hypothesis, the EDS analysis might not be as conclusive since it is often difficult to distinguish the grain boundary region that contains fewer acceptor dopants than the grain interior where only 2.5% Mg exists, in materials with volatile species such as Na and Bi. The ferroelectric domain observation differences and the correlation to the electrical conductivity could possibly be less ambiguous and thereby implies there must be a distinctive defect chemistry difference between the shell region around the grain boundary.

IV. CONCLUSIONS

In this paper, we demonstrate how the properties of BNT-15BT ferroelectric ceramic could be influenced by the sintering temperature coupling with Bi<sub>2</sub>O<sub>3</sub> stoichiometry perturbations. The batched excess Bi<sub>2</sub>O<sub>3</sub> will dope the BNT-BT material, rather than forming a secondary phase, in the calcined powder. When sintered at a high temperature, the excess Bi<sub>2</sub>O<sub>3</sub> remains doped on \(\overline{\mathbb{Z}}\) the A site, resulting in a decrease in T<sub>d</sub>. When sintered at a relatively low temperature, the excessive Bi<sub>2</sub>O<sub>3</sub> will be "released" to the grain boundary, enhancing the densification process. Accordingly, we identified some intriguing behaviors due to the manipulation of non-stoichiometry. At ambient temperature, the high temperature non-stoichiometry. At ambient temperature, the high temperature sintered BNT-15BT ceramic is the relaxor ferroelectric phase with considerably resistive grain boundary, whereas the low temperature sintered ceramic remains the normal ferroelectric phase with a much greater grain boundary conductivity. These observations are consistent with changes in activation energies controlling the ionic conductivity. A discontinuity is noticed and correlates to the depolarization temperature. In addition, a hypothetical mechanism for the resistive grain boundary is proposed, that is related to a sharply distinctive defect chemistry from the bulk of the grain.

ACKNOWLEDGMENTS

This work was supported by the National Science Foundation (NSF), as part of the Center for Dielectrics and Piezoelectrics under Grant Nos. IIP-1841453 and 1841466.

# **AUTHOR DECLARATIONS**

## **Conflict of Interest**

The authors have no conflicts to disclose.

# **Author Contributions**

**Zhongming Fan:** Conceptualization (equal); Data curation (equal); Formal analysis (equal); Investigation (equal); Methodology (equal); Writing - original draft (equal). Clive A. Randall:

.Downloaded from http://pubs.aip.org/aip/jap/article-pdf/doi/10.1063/5.0146059/17922298/214101\_1\_5.0146059.pdf

Funding acquisition (equal); Project administration (equal); Supervision (equal); Validation (equal); Writing - review & editing (equal).

# **DATA AVAILABILITY**

The data that support the findings of this study are available from the corresponding author upon reasonable request.

### **REFERENCES**

- <sup>1</sup>J. Rödel, W. Jo, K. T. P. Seifert, E.-M. Anton, T. Granzow, and D. Damjanovic, J. Am. Ceram. Soc. 92, 1153-1177 (2009).
- <sup>2</sup>H. Luo, H. Liu, S. Deng, S. Hu, L. Wang, B. Gao, S. Sun, Y. Ren, L. Qiao, and J. Chen, Acta Mater. 208, 116711 (2021).
- <sup>3</sup>M. Li, M. J. Pietrowski, R. A. De Souza, H. Zhang, I. M. Reaney, S. N. Cook, J. A. Kilner, and D. C. Sinclair, Nat. Mater. 13, 31-35 (2014).
- <sup>4</sup>Z. Fan and C. A. Randall, J. Mater. Chem. C 9, 10303–10308 (2021).
- <sup>5</sup>M. Li, H. Zhang, S. N. Cook, L. Li, J. A. Kilner, I. M. Reaney, and D. C. Sinclair, Chem. Mater. 27, 629-634 (2015).

- <sup>6</sup>A. Mishra, D. K. Khatua, A. De, B. Majumdar, T. Frömling, and R. Rajan, Acta Mater. 164, 761-775 (2019).
- <sup>7</sup>X. Liu, F. Li, P. Li, J. Zhai, B. Shen, and B. Liu, J. Eur. Ceram. Soc. 37, 4585-4595 (2017).
- <sup>8</sup>I.-T. Seo, S. Steiner, and T. Frömling, J. Eur. Ceram. Soc. 37, 1429–1436 (2017).
- <sup>9</sup>H. Qi, R. Zuo, X. Zhou, and D. Zhang, J. Alloys Compd. **802**, 6–12 (2019).
- 10 A. Mishra, G. Abebe, G. Jafo, G. D. Adhikary, and A. De, J. Mater. Sci.: Mater. Electron. 32, 12578-12593 (2021).
- <sup>11</sup>E. Aksel and J. L. Jones, J. Am. Ceram. Soc. **93**, 3012–3016 (2010).
- 12D. Hou, E. Aksel, C. M. Fancher, T.-M. Usher, T. Hoshina, H. Takeda, T. Tsurumi, and J. L. Jones, J. Am. Ceram. Soc. 100, 1330-1338 (2017).
- 13M. Makarovic, A. Bencan, J. Walker, B. Malic, and T. Rojac, J. Eur. Ceram. Soc. 39, 3693-3702 (2019).
- 14E. Salje, U. Bismayer, B. Wruck, and J. Hensler, Phase Transit. 35, 61–74 (1991).
- 15S. Lee, Z.-K. Liu, M.-H. Kim, and C. A. Randall, J. Appl. Phys. 101, 054119
- <sup>16</sup>Z. Fan, X. Liu, and X. Tan, J. Am. Ceram. Soc. **100**, 2088–2097 (2017).
- 17M. Vollman and R. Waser, J. Am. Ceram. Soc. 77, 235-243 (1994).
- 18D. Y. Wang and A. S. Nowick, J. Solid State Chem. 35, 325–333 (1980).